

Universidade Federal do Estado do Rio de Janeiro
Escola de Informática Aplicada
Bacharelado em Sistemas de Informação

Juliana Louback

Dermatologic Diagnosis through Computer Vision and Pattern Recognition

Rio de Janeiro, Brazil
2014

Juliana Louback

Dermatologic Diagnosis through Computer Vision and Pattern Recognition

**Monograph presented at the
Universidade Federal do Estado do Rio
de Janeiro, developed upon completion
of the Bachelor's in Information Systems.
Concentration: Computer Vision
Mentor: Sean Wolfgang Matsui Siqueira**

Rio de Janeiro, Brazil
2014
Juliana Louback

Dermatologic Diagnosis through Computer Vision and Pattern Recognition

Monograph presented at the Universidade Federal do Estado do Rio de Janeiro, developed upon completion of the Bachelor's in Information Systems.

Concentration: Computer Vision

Date of defense: June 12th, 2014

Result: _____

Examining Committee

John Doe

Universidade Federal do Estado do Rio de Janeiro

John Doe

Universidade Federal do Estado do Rio de Janeiro

John Doe

Universidade Federal do Estado do Rio de Janeiro

I would like to dedicate this monograph to prof. Rob Fergus who first introduced me to the field of Computer Vision; and Dr. Jefferson Braga Louback, my father, whose devoted efforts in enabling access to medical care have long inspired my admiration.

Acknowledgements

I would like to express my gratitude to my mentor, prof. Sean Wolfgang Matsui Siqueira without whose guidance this article would never have been completed; prof. Rob Fergus, prof. Richard Staunton and prof. Li Ma who provided invaluable advice regarding the development of the algorithms used; Tom Gibara for his most effective implementation of the Canny Corner Detector and Yuri Pourre for permitting the use of his Quick Hull algorithm; my 6 siblings Piero, Daniela, Paula, Natali, Davi and Larissa who I am certain did all within their power to keep the noise level down to a minimum so as not to hinder my work; my mother Sylvia for her unwavering support and confidence in my ability; Dr. Jefferson B. Louback, Dr. Ricardo Barbosa Lima and Dr. Carlos José Martins who contributed with curated images of skin lesions and acted as consultants for the medical aspects of the monograph, which are beyond my domain of knowledge.

Summary

This project endeavors to quantify the effectiveness of computer vision and pattern recognition techniques in the diagnosis of melanoma. In dermatology, the ABCD guide is a widely known method for the detection of a malignant melanoma. This guide is a set of four identifying traits: Asymmetry; Border irregularity; Color changes; Diameter greater than 6 mm. Over the past decade, various algorithms that examine digital images of skin lesions to detect the presence of malignant melanomas have been developed and tested. The algorithms use the analysis of border irregularity to provide a diagnosis. The most recent of these was developed by Dr. Richard Staunton of the University of Warwick and Li Ma of the Hangzhou Dianzi University and presents the best results with regards to accuracy and performance. This algorithm uses 13 features based on a set of statistical and geometric irregularity descriptors. The experiment proposed is first to evaluate the images using only a geometric descriptor for border irregularity and compare its effectiveness to Ma and Staunton's multi-descriptor analysis. Next, a metric is developed to represent the remaining 3 categories of the ABCD melanoma diagnosis criteria to be used in conjunction with the Border Irregularity metric. and increase levels of accuracy. A second round of evaluations is performed to ascertain the influence of the additional metrics. The algorithms are run on a labeled dataset of 480 images and the specificity, the number of accurately diagnosed images of melanoma, is calculated. Sensitivity is of lesser importance as incorrectly classifying a non-malignant lesion as malignant presents less critical consequences as overlooking a malignant lesion. However, in both cases, sensitivity is also taken into consideration in the final evaluation. In conclusion, a practical application of these techniques is explored with the intent of providing solutions to the prevalent issue of limited access to medical care. The process, maturation and findings of the undertaking are detailed in this monograph.

List of Tables

Table 1 - Comparison of classification performances.....	18
Table 2 - Summary of Key ABCD(E) Sensitivity and Specificity Studies.....	19
Table 3 - Final feature selection.....	27

List of Figures

Figure 1 - Mean dermatologist density among US counties.....	11
Figure 2 - Asymmetry: Malignant and benign example.....	13
Figure 3 - Border Irregularity: Malignant and benign example.....	14
Figure 4 - Color Variegation: Malignant and benign example.....	14
Figure 5 - Diameter Size: Malignant example.....	15
Figure 6 - Wavelet decomposition tree.....	22
Figure 7 - Contours after wavelet reconstruction.....	25
Figure 6 - Image rotation example.....	15
Figure 7 - Comparison of optimal and Gaussian operator.....	16
Figure 8 - Threshold performance comparison.....	18
Figure 9 - Threshold performance on image of melanoma.....	18
Figure 10 - Quick Hull generated polygon containing the skin lesion.....	21
Figure 11 - Summary of Symmetry Detector results.....	22
Figure 12 - Comparison of metric on malignant and nonmalignant lesions.....	23

Index

1. INTRODUCTION	
1.1 The Scope of Analysis	10
1.2 Monograph Structure	12
2. FUNDAMENTALS	
2.1 ABCD Criteria.....	13
2.2 Prior Art.....	16
3. PROPOSAL	
3.1 Proposed Objectives.....	19
4. IMPLEMENTATION	
4.1 Ma and Staunton's algorithm.....	21
4.2 Canny Corner Detector.....	28
4.3 AB*CD Metrics	
4.3.1 Asymmetry metric.....	32
4.3.2 Border irregularity metric.....	35
4.3.3 Color change metric.....	36
4.3.4 Diameter size.....	37
4.4 Image Pre-processing.....	39
5. ANALYSIS	
6. CONCLUSION	

1. INTRODUCTION

The first chapter of this monograph provides a high-level understanding of the motivation behind this research. The scope of analysis is defined in order to demonstrate the importance and potential value which may be added followed by a brief description of the structure of the monograph to facilitate comprehension.

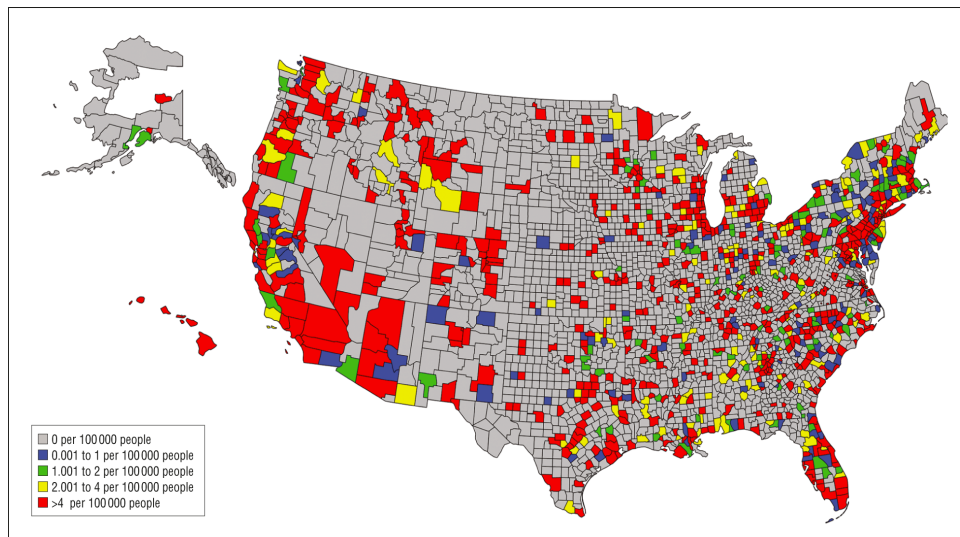
1.1 The Scope of Analysis

There is a noted undersupply of dermatologic services worldwide, common to both developing and developed countries. The effects of such a deficit in the workforce is clearly shown in the excessive mean wait times for appointment availability; it was recently discovered that a patient must schedule a dermatologic consult an average of 33 days in advance in the United States[13] and 26 days in advance in Brazil[20].

Estimates of the current number of practicing dermatologists range from 8,000 to 8,5000 in the United States and approximately 6,000 in Brazil. This is a pitifully inadequate number of professionals to cater to the 300 million Americans and 200 million Brazilians. Researchers from the Case Western Reserve University and Yale University performed a study that showed the direct correlation between dermatologist density and melanoma mortality rates[2]. This finding is already significant in countries like the United States and Brazil where there is an estimated ratio of 35,000 people per dermatologist and even more severe in countries like South Africa with 3 to 4 million people per dermatologist[19].

Dermatology specialists are mainly based in capitals and major cities, limiting greatly the access to a dermatologist (*See Figure 1*). Technology has previously been applied to other fields to overcome geographical barriers; this project evaluates the efficiency and effectiveness of a series of computerized methods that may be applied to the dermatologic diagnosis process, in an effort to assuage this disequilibrium in supply and demand.

Figure 1 - Mean dermatologist density among US counties, 2002-2006



Source: ANEJA, S; ANEJA, S; BORDEAUX J.S. [2]

In the field of dermatology, the vast majority of medical cases are diagnosed visually, as the affected regions are at least partially superficial. According to CDC's National Ambulatory Medical Care Survey in 2009, the top 5 reasons given by patients for visiting dermatologists were actinic and seborrheic keratosis, benign neoplasm, acne, malignant neoplasms and contact dermatitis and other eczema. These conditions account for near 80% of medical consults. Of the 5 listed, 4 can be diagnosed through a visual examination.

The National Cancer Institute defines a neoplasm as an abnormal mass of tissue that results when cells divide more than they should or do not die when they should. A neoplasm can also be called a tumor and may be benign or malignant. Melanoma is a malignant neoplasm that begins in melanocytes commonly on skin but may also begin in other pigmented tissues such as in the eye or in the intestines. The scope of this project will be limited to skin melanoma diagnosis through digital image analysis, using binary classification algorithms with melanoma/non-melanoma as prediction categories.

Within the ambit of neoplasm diagnosis, there are certainly more options than melanoma and non-melanoma. Among the malignant neoplasms there are non-melanoma skin cancers, consisting primarily of basal cell carcinomas and squamous cell carcinomas[27]. Multinomial classification could be employed to

include these varieties of neoplasms in the analysis performed, yet would add significant complexity. On that account, it was decided that a more conservative approach would be most adequate for the initial stages of this study, limiting the classifier algorithm to two categories. As melanomas are more commonly fatal than non-melanoma malignant neoplasms[27], melanoma diagnosis was defined as the focus of the research.

Skin melanoma may be diagnosed through a visual examination performed by a dermatologist. The definitive diagnosis is usually rendered on pathologic evaluation of a lesional skin biopsy specimen[26]. The potential malignancy is recognized during the initial (visual) examination, following which a biopsy is performed to confirm the prognosis. As such, although image analysis systems are not to be relied upon for a complete diagnosis, they may be a viable solution to perform a triage and prioritize examinations.

1.2 Monograph Structure

The monograph is organized into 6 chapters, these being Introduction, Fundamentals, Proposal, Implementation, Analysis and Conclusion. The first chapter describes the domain of the issue, that of automated melanoma detection, as well as a high level description of the solution proposed. The introductory chapter also provides a basic explanation of the medical terms employed. Fundamentals discusses previous studies in related fields and how prior findings will be included in this monograph. Proposal details the solution to be developed, describing the components and logic pertaining to the image analysis system. The Implementation chapter documents the development of the solution, exhibiting the intermediate results obtained. Analysis outlines the execution of the image analysis system, resulting in a dataset to be used in the classifier system. Conclusion will summarize the performance of the classifier system, its findings and ongoing work.

2. FUNDAMENTALS

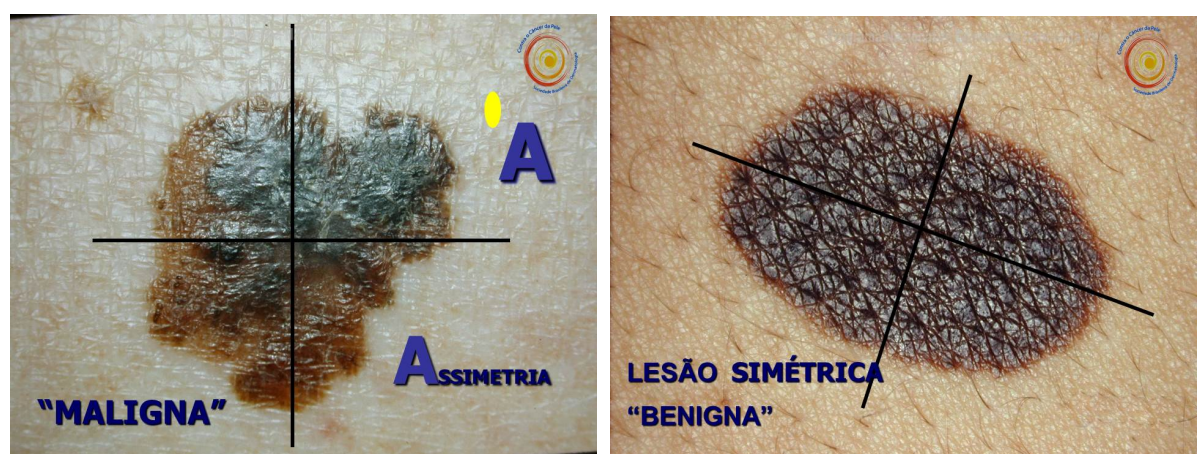
The following chapter details the identifying traits used to detect melanoma in a visual examination and a description of previous studies related to the employment computer vision methods and algorithms for dermatologic diagnosis.

2.1 ABCD Criteria

The ABCD acronym was first coined in the article *Early Detection of Malignant Melanoma: The Role of Physician Examination and Self-Examination of the Skin* [7] written by Dr. Robert Friedman, Dr. Darrell Rigel and Dr. Alfred Kopf of the New York University School of Medicine in 1985. This article was prepared in conjunction with the Task Force on Preventive Dermatology of the American Academy of Dermatology and the American Cancer Society; the ABCD Criteria was meant to be used by both the lay public and health professionals to assist in the early detection of melanoma and consequently increase survival rates[7]. ABCD stands for Asymmetry, Border Irregularity, Color variegation, and Diameter generally greater than six mm[7].

Asymmetry

Figure 2 - Asymmetry: Malignant and benign example



Source: prof. Ricardo Barbosa Lima of UNIRIO

“Unlike benign pigmented lesions, which are generally round and symmetrical, early malignant melanomas are usually asymmetrical” [7] (Figure 2)

Border Irregularity

Figure 3 - Border Irregularity: Malignant and benign example

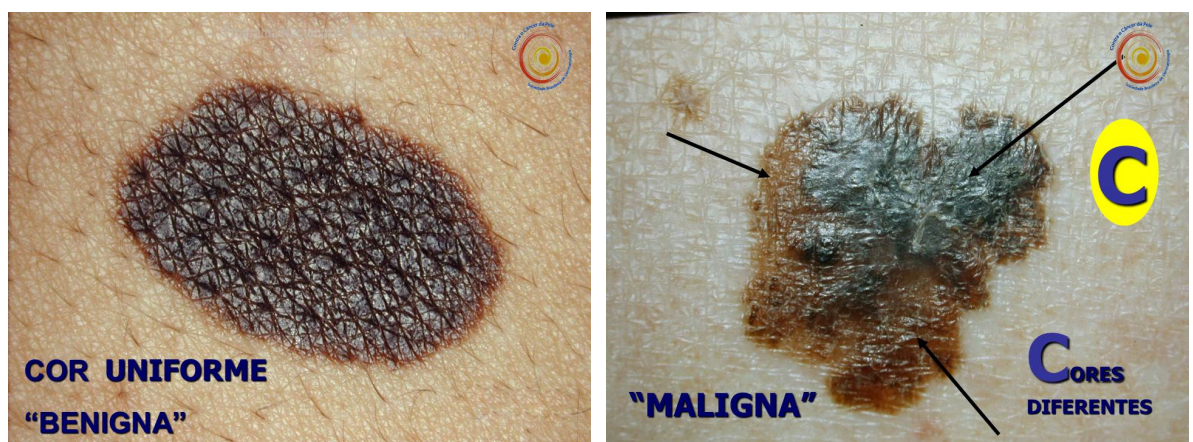


Source: prof. Ricardo Barbosa Lima of UNIRIO

"Unlike benign pigmented lesions, which generally have regular margins, the borders of early malignant melanomas are usually irregular. " [7] (Figure 3)

Color Variegation

Figure 4 - Color Variegation: Malignant and benign example



Source: prof. Ricardo Barbosa Lima of UNIRIO

"Unlike benign pigmented lesions, which are generally uniform in color, macular malignant melanomas are variegated, ranging from various hues of tan and brown to black, and sometimes intermingled with red and white." [7] (Figure 4)

Diameter greater than six mm

Figure 5 - Diameter size: Malignant example



Source: prof. Ricardo Barbosa Lima of UNIRIO

“Unlike most benign pigmented lesions, which generally have diameters less than six mm, the diameters of macular malignant melanomas when first identified are often more than six mm.” [7] (Figure 5)

It is possible that the fourth trait, ‘Diameter greater than 6 mm’, may not be as symptomatic as the remaining 3 traits. A study performed in 2004 by Dr. Friedman, Dr. Rigel, and Dr. Kopf and other colleagues of the New York University School of Medicine and the Sydney Melanoma Unit suggested a reexamination of the ABCD criteria in view of data attesting to the existence of melanoma with a diameter smaller than 6 mm[1]. Although the conclusion reached was that the available data did not support a lowering of the 6mm threshold, the study emphasizes the need to use the ABCD traits in conjunction as there are cases of small-diameter melanomas.

During the same study by Kopf and his colleagues, detailed in the article *Early Diagnosis of Cutaneous Melanoma: Revisiting the ABCD Criteria*[1] it was concluded that an additional criterion ‘E’ should be added to the acronym, representing the evolution of pigmented lesions. It is said that “Physicians and patients (...) should be attentive to changes (evolving) of size, shape, symptoms (itching, tenderness), surface (especially bleeding), and shades of color.” [1] However, this additional criterion cannot be well represented by a digital image and as such will not be included in this experiment.

2.2 Prior Art

In dermatology, the ABCD guide is a widely known method for the identification of a malignant melanoma[22]. This guide is a set of 4 traits common to malignant melanomas: Asymmetry; Border irregularity; Color variegation; Diameter greater than 6 mm. Extensive research has been performed regarding the analysis of border irregularity in relation to melanoma diagnosis. Some of these studies indicate that the diagnosis of malignant melanomas can be based on the analysis of the shape of the lesion alone[15]. Many of said studies which present most noteworthy results make use of Wavelet Transform Analysis.

The term ‘wavelet’ (originally in French, ‘ondelettes’) was first coined in 1982 by the French geophysicist Jean Morlet[21], one of the pioneers in Wavelet Analysis. Morlet sought an alternative to the short time Fourier Transform[6] which is a modification of the Fourier transform to permit the analysis of non-stationary signals. Assuming a time-domain signal as the raw signal, a Fourier transform could be used to obtain the Frequency Spectrum. The Fourier Transform contains no information with regard to time, ergo the need for the short time Fourier Transform for a non-stationary signal. The short time Fourier Transform performs sequential Fourier Transforms on segments of the signal which are (near) stationary.

The disadvantage of the short time Fourier transform lies in the necessary sacrifice of either good time resolution or good frequency resolution according to the window used in the kernel function. To gain good time resolution in the high-frequency components as well as good frequency resolution in low-frequency components in a single transform, Morlet proposed an alternate method for generating the transform functions. In sum, instead of using a window of changeable width to perform a Fourier Transform on a time interval of the signal, Morlet took a windowed cosine wave whose width was shifted to adjust to low or high frequencies and shifted these functions in time as well[6]. As a result, the transform functions relied on two parameters: the time location and scale, which represents the frequency. Since then, the basis Wavelet theory has been built upon by a series of scientist who have explored its applications in a variety of fields.

There are two main trends in the use of Wavelet Transforms[12], the Continuous Wavelet Transforms and the Discrete Wavelet Transforms. The

Continuous Wavelet Transforms (CWT) consists of an analysis window (function) of varying scale being shifted not only in scale but in time, obtaining the signal product and integrating over all times. In the Discrete Wavelet Transform (DWT) low and high pass filters are used to analyze low and high pass frequencies, respectively, removing redundancy present in the CWT. The CWT's redundancy does have a purpose, emphasizing traits and adding readability. The DWT reduced computational time due to reduced redundancy may be the cause of its greater popularity among engineers[12].

A study performed by K.M. Clawson of the University of Ulster uses the Harmonic Wavelet Transform to analyze lesion border irregularity, claiming maximum classification accuracy of 93.3% with 80% sensitivity[5] when tested on 30 cutaneous lesions. The Harmonic Wavelet Transform was developed by David Newman in 1993[23]. This name may be derived from its frequency resolution, "confined exactly to an octave band so that it is compact in the frequency domain"[23]. However, this fixed resolution throughout the frequency band inhibits the separation of signal components[17] which in turn hinders the distinction of structural and textural irregularities. It is the structural irregularity that has clinical importance for melanoma diagnosis[17]. In 2012, Li Ma of the Hangzhou Dianzi University and Richard C. Staunton of the University of Warwick circumvented this difficulty by using a Discrete Wavelet Transform to single out the structural components[17]. Their study involved 134 images of skin lesions; of these 72 were of melanomas and 62 of moles. The most significant distinction between melanomas and moles is that moles are benign neoplasms whereas melanomas are malignant neoplasms. The algorithm could be summarized as a two-step procedure: multi-scale wavelet decomposition of the extracted contour followed by the selection of significant sub-bands.

Wavelet decomposition was used to extract the structure from the contour which were then modeled as signatures with scale normalization to give position and frequency resolution invariance. Energy distributions among different wavelet sub-bands were then analyzed to extract those with significant levels and differences to enable maximum discrimination. A set of statistical and geometric irregularity descriptors were applied at each of the significant sub-bands, followed by an effectiveness evaluation to select which descriptors contribute to an accurate

diagnosis. The effectiveness of the descriptors was measured using the Hausdorff distance between sets of data from melanoma and mole contours. The best descriptor outputs were input to a back projection neural network to construct a combined classifier system. This algorithm will be described in greater detail in the implementation chapter of the monograph.

Li and Staunton's optimum combination resulted in an area under ROC curve of 0.89 with 90% specificity and 83% sensitivity, similar to Clawson's findings. These results were obtained from a small data set consisting of 18 images, 9 of which were of melanomas and 9 of moles. With a larger training set of 67 images (31 moles and 36 melanomas), these numbers fell to 0.83 ROC with 83% sensitivity and 74% specificity, which signifies that a greater number of non-malignant moles would be classified as melanomas.

Table 1 - Comparison of classification performances

Scheme	Specificity	Sensitivity	Area of ROC
Single scale features with small sample set	0.64566	0.69444	0.69534
Single scale features with large sample set	0.87903	0.55556	0.75179
Original multi-scale features with small sample set	0.83871	0.69444	0.81541
Original multi-scale features with large sample set	0.80645	0.69444	0.81989
Selected multi-scale features with large sample set	0.74194	0.83333	0.83333
Selected multi-scale features with small sample set	0.90323	0.83333	0.89068

Source: MA, L.; STAUNTON, R.C. [17]

These findings are incredibly significant given the high levels of accuracy and reduced computational cost. It is of interest to analyse this algorithm in conjunction with remaining three features of the ABCD criteria: asymmetry, color change and diameter size.

3. PROPOSAL

The proposed solution is described in greater detail as well as the expected results. Methods of evaluation will also be presented.

3.1 Proposed Objectives

This study will implement and evaluate a multi feature image analysis system in an effort to gauge the effectiveness of its employment in melanoma diagnosis. It will be necessary to first identify the significance of each feature in the classification of skin lesions and determine what combination of features provide the most accurate results.

Li Ma and Richard C. Staunton have generously agreed to the inclusion of their algorithm in this experiment. However, the original software for the algorithm detailed in the article *Analysis of the contour structural irregularity of skin lesions using wavelet decomposition*[17] could not be recovered. To circumvent this contretemps, the algorithm was reimplemented in consultation with Ma and Staunton as part of the study.

The system is divided into two parts; the first is Ma and Staunton's algorithm, which uses border irregularity to determine malignancy. Border irregularity is one of four identifying traits used in the diagnosis of melanoma. Studies have shown that accuracy levels vary according to the traits included in performing diagnosis, both singly and in combination (See Table 1). Therefore the second part of the system consists of three algorithms to formulate additional metrics for the remaining identifying traits, these being Asymmetry, Color change and Diameter size.

Table 1 - Summary of Key ABCD(E) Sensitivity and Specificity Studies

Table 1. Summary of Key ABCD(E) Sensitivity and Specificity Studies					
Source	Total No. of Lesions	No. of Melanomas	Criteria Tested	Sensitivity, %	Specificity, %
Thomas et al. ⁴ 1998*	1140	460	A	57	72
			B	57	71
			C	65	59
			D	90	63
			E	84	90
			≥1 Criterion	97	36
			≥2 Criteria	89	65
			≥3 Criteria	66	80
			≥4 Criteria	54	94
			All 5 criteria	43	100
McGovern and Litaker, ¹⁰ 1992	192	6	BCD criteria applied jointly	100 (95% CI, 54-100)	98 (95% CI, 95-99)
Healsmith et al. ³ 1994†	165	65	≥1 of the ABCDEs	92 (95% CI, 82-96)	Not reported

Abbreviations: ABCD, Asymmetry, Border irregularity, Color variegation, Diameter greater than 6 mm; CI, confidence interval
*The authors used lesion diameter 6 mm or greater as the cutoff for this study and tested an E criterion (for horizontal enlargement).

†The authors tested E for elevation.

Source: Thomas, L. et al. [27]

Staunton and Ma's algorithm uses 13 features based on a set of statistical and geometric border irregularity descriptors. The simple geometric descriptor will be compared with Ma and Staunton's algorithm to measure the added accuracy of the 13 features used. Subsequently the three descriptors for Asymmetry, Color change and Diameter size will be included in a combined algorithm. As stated by Kopf and his colleagues, "It should be emphasized that not all melanomas have all 4 ABCD features. It is the combination of features (eg, ABC, A+C, and the like) that render cutaneous lesions most suspicious for early melanoma." [1] If this is true of in-person examinations performed by a specialist, it may also be implied of computer vision analysis.

A total of 17 features are attributed to each image of a skin lesion, recorded in the data set which is run through a Back Propagation Neural Network to classify each instance as melanoma or non-melanoma. The back propagation (BP) neural network algorithm is a multi-layer feedforward network trained according to error back propagation algorithm and is one of the most widely applied neural network models[11]. This model was used in the development of Ma and Staunton's algorithm and will continue to be used to maintain consistency. The algorithm is measured for sensitivity and specificity levels in addition to overall accuracy.

Sensitivity will be given a higher priority than specificity, as the correct identification of a malignant or potentially malignant tumor is of greater consequence than a false positive diagnosis, within reasonable levels. However, the inconvenience of an incorrect positive diagnosis is by no means irrelevant, therefore despite specificity being a secondary priority, ideally the solution proposed will result in no less than 80% specificity.

Once the algorithms have been compared and measured for accuracy, a proposal for practical application will be formulated. As 100% accuracy is an unrealistic expectation and the biopsy necessary for a definitive diagnosis, specialist confirmation remains necessary. This project will study whether it is feasible and advantageous to incorporate computer vision algorithms to current traditional diagnosis methods.

4. IMPLEMENTATION

This chapter details the development of the algorithms used in this experiment. Difficulties encountered and modifications to the original plan of action are included due to their contribution to the overall knowledge acquired and possibly influence over final results. First the re-implementation of Ma and Staunton's Border Irregularity algorithm[17] is described, followed by the implementation of algorithms for the simple geometric border irregularity metric and the remaining metrics: asymmetry, color change and diameter size.

4.1 Ma and Staunton's Algorithm

Li Ma and Richard C. Staunton of the Hangzhou Dianzi University and Warwick University[17] developed an algorithm to analyze skin lesion border irregularity using multi-scale wavelet decomposition. As the code for the algorithm was not recovered, it was necessary to re-implement it so as to include it in this study. The code was originally written in Matlab, a high-level technical computing language and interactive environment for algorithm development. However, due to budget limitations the algorithm was re-implemented in Octave, an open source alternative comparable to and generally compatible with Matlab. The algorithm is roughly divided into two phases: Wavelet decomposition of a lesion contour and Sub-band descriptions of contour structural components. Following is a summarized and commented description of the algorithm extracted from the article *Analysis of the contour structural irregularity of skin lesions using wavelet decomposition*[17].

1. Wavelet decomposition

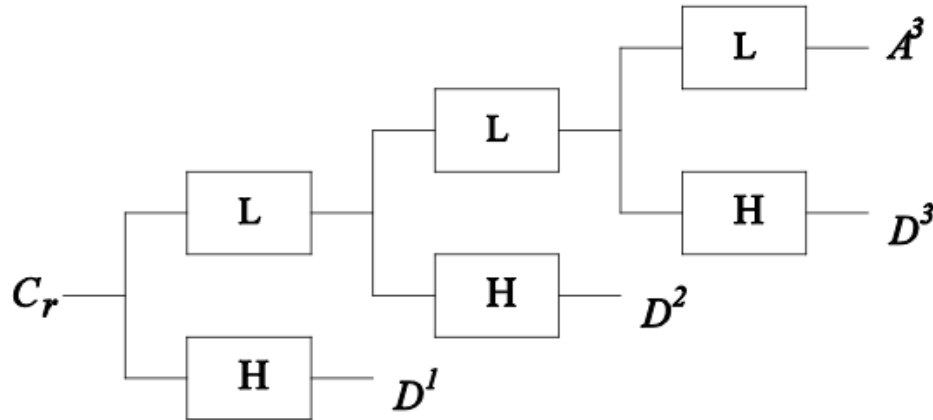
1.1. Represent the contour in 1D signal

The contour of a skin lesion in an image is described by the points $C = \{x_1, y_1, x_2, y_2, \dots, x_N, y_N\}$. [These points were obtained using a Canny edge detector function.] To represent this 2D data as 1D, the contour is modeled as a signature $C_r = \{r_1, r_2, \dots, r_N\}$ where the radial distance from the geometric center $r_i = \sqrt{(x_i - x')^2 + (y_i - y')^2}$, $i = 1, 2, \dots, n$ and (x', y') is the coordinate of the geometric center of the closed contour.

1.3 Wavelet decomposition

Wavelet decomposition is a powerful tool for multi-scale signal analysis. By using a pair of low-pass and high-pass filters [the lesion contour signature] is decomposed into approximation and detail coefficients with the approximations feeding into the next level of decomposition, and thus creating a decomposition tree. The tree structure of such a 1D wavelet decomposition is shown in [Figure 6].

Figure 6 - Wavelet decomposition tree



Source: MA, L.; STAUNTON, R.C. [17]

The approximate and detail coefficients at scale i are given by $A_i = \{a_1^i, a_2^i, \dots, a_M^i\}$ and $D_i = \{d_1^i, d_2^i, \dots, d_M^i\}$ respectively where $M = N/2^i$. [It is important to recall that the Discrete Wavelet Analysis uses windowed cosine wave whose width is successively modified. The width, also known as compression of said wave is represented by a scale[6]. The smaller the scale, the more narrow the wave ergo the higher the frequency. The inverse is also true; the greater the scale, the wider the wave ergo the lower the frequency.] As the scale increases, the approximate coefficients are further decomposed into low and high frequency components at the next higher scale. Generally the textural components of a contour occupy the lower scale, higher frequency bands, with the energy distributed evenly between bands to give a relatively small total energy within each. However the structural components generally have a larger energy and occupy the lower frequency bands. By using wavelet decomposition to level s , an original contour signature C_r is transformed to a series of sub-band signals $A^s, D^s, D^{s-1}, \dots, D^1$ covering the whole signal frequency space at $[0, 1/2^s f_{max}], [1/2^s f_{max}, 1/2^{s-1} f_{max}], \dots, [1/2^1 f_{max}, 1/2^0 f_{max}]$, $i=s, s-1, \dots, 2, 1$ and f_{max} is half the sampling frequency. This represents a concatenation of the frequency bands from the lowest to the highest. The task is to identify at which decomposition levels the structural components of a lesion contour can be extracted and which sub-bands in the frequency domain are significant for

distinguishing moles and melanomas.

2. Sub-band descriptions of contour structural components

[The Discrete Wavelet Transform was selected for use over the Fast Fourier Transform because it presents the capability of confining signal components to dyadically increasing width frequency bands with different resolutions.

2.1 Significant sub-band selection

To obtain just the contour's structural components [ignoring the less relevant textural components], several lower frequency sub-bands need to be identified from which to reconstruct that portion of the original contour using both multi-scale approximate and detail coefficients. The evaluation of the significant sub-band range was performed between each of the sample sets by [Hausdorff] distribution analysis at each level of wavelet decomposition. When analyzing the decomposition of a contour signal, the total energy at any decomposition level indicates the significance of that sub-band frequency to the original signal. The energy of a wavelet sub-band D_j is defined as

$$E_j = \sum_i (D_j^i)^2 \quad j = 1, 2, \dots n$$

2.2 Procedure for investigating significant sub-band selection

An algorithm was developed to identify those sub-bands which enabled the largest discrimination between moles and melanomas. [This was done with] a set of p benign mole contours and a set of q melanoma contours

Step 1: For a preset maximum level of wavelet decomposition n , calculate the wavelet energy for every contour [from the set of moles and melanomas]. Then calculate the energy of each sub-band [obtained from the wavelet decomposition to level n].

Step 2: Form energy sets from the individual energies calculated for each transformed benign [mole] and melanoma contour at each sub-band.

Step3. Compute the [Hausdorff Distance] value between energy sets of moles E_b and melanomas E_m for each band. This measures the discrimination between the two classes for each sub-band.

Step 4. Plot the distribution of [the Hausdorff Distance] with respect to [each] sub-band. The sub-bands with the highest HD are considered as the most significant and used in the final classification.

2.3 Extraction of the structural component of a lesion contour

Based on the theory of wavelet reconstruction, the structural component of a lesion contour is given by combining the significant coefficient groups from A^s , D^s , D^{s-1} , ... D^1 where the original decomposition was stopped at level s . The decomposed detail sub-bands need to be divided into high-scale (low-frequency) and low-scale (high-frequency) groups using a threshold s_t so that:

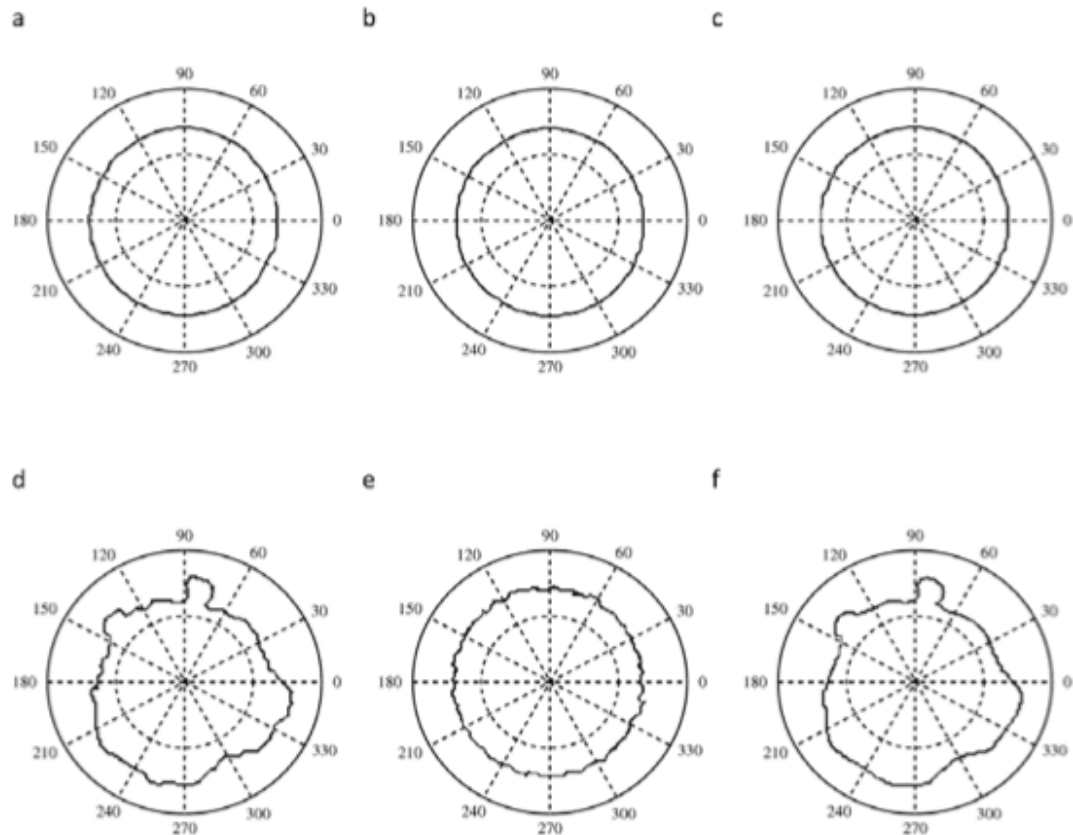
$$C_s = \{ A^s + D^s + D^{s-1} + \dots + D^{s_t} \}$$

$$C_t = \{ D^{s-1} + D^{s-2} + \dots + D^1 \}$$

Where C_s contains lower-frequency information and represents the structural component of the contour, and C_t contains higher-frequency information and represents the textural component. Choosing both s and s_t are difficult tasks, as a large s generates many narrow sub-bands close to zero frequency. Although these will contain structural information that will be relatively free of textural irregularity, there is an extra cost in increased computational complexity. A small s can lead to structural contours contaminated with textural irregularity. The value of s_t chosen is crucial to obtain useful structural and textural contour information. The significant sub-band selection process described in Section [2.2] was run on the test data [which] lead to the straightforward selection of a single, general value for s_t . [The frequency bands that contained significant discrimination information were sub-bands D^6 to D^9 , and as such were selected as the significant levels.]

It is simple to reconstruct the structural components of the contour after the significant levels in the wavelet decomposition stack have been determined. [Figure 7] shows the extracted contours of a mole (a,b,c) and a melanoma (d,e,f), where [Figure 7 a) and d)] are the original contours, [Figure 7 b) and e)] are the corresponding contours reconstructed from A^9 and D^1 to D^5 . The approximation coefficient, A^9 has been included to give the basic structure of the contour onto which the more complex textural part has been superimposed. [Figure 7 c) and f)] are reconstructed from A^9 and D^6 to D^9 ($s = 9$, $s_t = 6$), that is the boundaries representing the structural portion of the original lesion. With the textural information removed, these have the property of the highest discrimination between different lesion classes. In the remainder of the paper these significant sub-bands will be referred to as the structural sub-bands.

Figure 7 - Contours after wavelet reconstruction



Source: MA, L.; STAUNTON, R.C. [17]

Observing Figure 7, one can easily note the striking difference in discrimination based on textural and structural components. The contours in b) and e) reconstructed from the textural components of the mole and melanoma respectively present an almost imperceptible difference and would add very little to a classification system. In contrast, the contours c) and f) which were reconstructed from the structural components are clearly distinctive. As the significant sub-band selection was performed during Ma and Staunton's study, leading to the selection of a single value for s_t , with the approval of Li Ma, this phase of the algorithm was bypassed; the re-implementation uses the selected s_t value directly.

Once the significant sub-bands were identified, it was possible to calculate the series of border irregularity measures the algorithm is comprised of. Ma and Staunton used 7 different measures, these being either statistical or geometric based[17]. The measures and their respective formulas are listed below as described in Ma and

Staunton's article:

3.1 Statistical measures

Together with the mean(1) and variance of the energy of D^j at each significant level, the following features related to contour irregularity were defined:

$$1. \text{ Entropy of wavelet energy, } w_j = - \sum_{i=1}^N p_i^j \log(p_i^j) \quad (2)$$

where $p_i^j = E_i^j / E^j$ is the energy probability of the i th component of D^j , E^j is the total

energy of the coefficients in band j as calculated by $[E_j = \sum_i (D_j^i)^2 \quad j = 1, 2, \dots, n]$,

and $E_i^j = |D_i^j|^2$. The energy entropy measures the magnitude of signal fluctuations.

2. Ultimate width. For any signal $X = \{x_1, x_2, \dots, x_N\}$, the ultimate width is defined as

$$\text{width} = \frac{2\sigma}{\mu} \quad (3)$$

Where μ and σ are the mean and variance of signal X . A large width indicates sharp variations.

3.2 Geometric based irregularity measures

At each significant level j , a supposed structural component C_j , $s \geq j \geq s_t$ of a contour is reconstructed from the wavelet coefficients, $C_j = A^s + D^s + \dots + D^j$. In addition to a simple variance measure (4), the other irregularity measures of the reconstructed contours are evaluated as:

$$\text{Radial Deviation, } RD = \frac{1}{N} \sum_{i=1}^N |(r_i - \bar{r})| \quad (5)$$

where \bar{r} is the mean radius of the contour signature.

$$\text{Contour Roughness, } R_o = \frac{1}{N} \sum_{i=1}^N |r_i - r_{i+1}| \quad (6)$$

$$\text{Irregularity Measure, } IM = \frac{\text{Area}(C_j \oplus S_s)}{\text{Area}(S_s)} \quad (7)$$

where S_s is reconstructed from the approximate data, A^s , at the significant level s , and \oplus is the exclusive-or operator.

With the seven irregularity measures described above and the four significant sub-bands (D^6 , D^7 , D^8 , and D^9), there would be a total of 25 features: measures (1) to

(6) for each of the four significant sub-bands (24 features thus far), and IM (irregularity measure 7) at the threshold scale s_r . However, these features were filtered to remove redundancy. This was done by a correlation analysis followed by performance based feature selection. Correlation analysis computes the correlation coefficient for a pair of features t_i, t_j , from a feature vector $F = \{t_1, t_2, \dots, t_n\}$ and a sample set $S = \{x_1, x_2, \dots, x_m\}$. A large correlation coefficient indicates redundancy[17]. The performance based feature selection requires calculating the probability distribution of each feature's contribution to a correct classification, tested on both benign and malignant sample sets. The accumulated probability is found, then each feature is verified with an established classification error threshold[17].

Once the correlation analysis and the performance based feature selection was executed, 12 of the original 25 features were removed due to redundancy. The remaining 13 features are Average Energy(1) for sub-band 6-8; Wavelet Entropy(2) for sub-bands 6-9; Ultimate Width(3) for sub-bands 6, 7 and 9; Radial Deviation(5) for sub-band 6; Contour Roughness(6) for sub-band 7; and Irregularity Measure(7) for sub-band 6. The selected and eliminated features are displayed in Table 3.

Table 3 - Final feature selection

Sub-band	Average energy	Wavelet Entropy	Ultimate Width	Variance	Radial deviation	Contour roughness	Irregularity measure
6	✓	✓	✓		✓		✓
7	✓	✓	✓		✓		
8	✓	✓					
9		✓	✓				

Table in accordance to information from MA, L.; STAUNTON, R.C. [17]

Similarly to the significant sub-band selection procedure, as the redundant features were previously identified during Ma and Staunton's study, with the approval of Li Ma, the identification of redundant features was not done; the re-implementation uses the final feature selection directly.

4.2 Canny Corner Detector

The first step is to single out the skin lesion from the image. In doing so, the amount of data to be processed reduced considerably. Furthermore, considering the fact that Border Irregularity is one of the four identifying traits of melanoma, extracting the border of the lesion is essential to the success of the ‘B’ component of the ABCD Linear Regression algorithm. For this phase of the process, Tom Gibara’s Java implementation of the Canny Corner Detector[8] algorithm is used. The algorithm, detailed in the monograph *A Computational Approach to Edge Detection* by John Canny, is notably effective and as such it is ubiquitously used. It can be resumed in four main steps: Image filtering; gradient magnitude computing; Non-maximum suppression and hysteresis thresholding to trace the edges.

1 - Image filtering

The Canny Edge detector is highly susceptible to noise; the first step in the algorithm is filtering the image to reduce the misleading effect of noise pixels through a step edge detector. Canny calculated the optimal filter for this task, named ‘Filter number 6’ in his article[3]. However, he observed that although the first derivative of Gaussian operator performed approximately 20% worse than the optimal operator in the performance evaluations, this difference is hardly noticeable when visualizing their effects on real images. As the optimal operator requires much more computational effort than the first derivative of the Gaussian, the image is convolved with a Gaussian filter to obtain the desired noise reduction.

Figure 6 - Comparison of optimal and Gaussian operator.

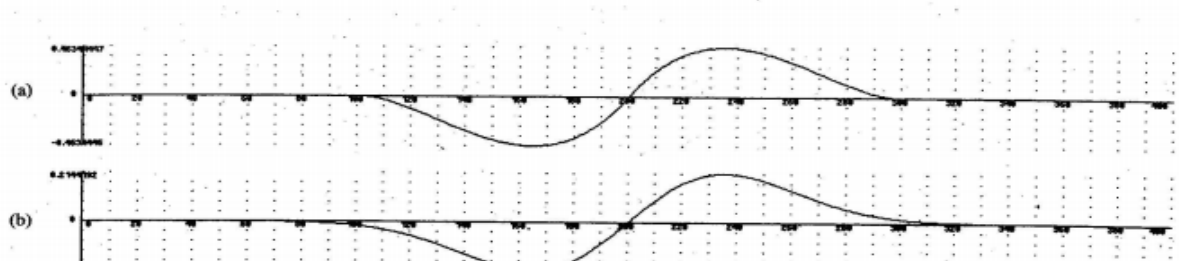


Fig. 6. (a) The optimal step edge operator. (b) The first derivative of a Gaussian.

Source: CANNY, John. [2]

2 - Gradient magnitude computing

The gradient of an image indicates the direction of a rapid change in intensity and as such provides information regarding the orientation of the edge, whether it is horizontal, vertical or diagonal. In a two dimensional coordinate system as is this case, the gradient is given by

$$\nabla f = \frac{\partial f}{\partial x} + \frac{\partial f}{\partial y}$$

the vector composed of the partial derivatives of f . A horizontal gradient is given by

$$\nabla f = 0 + \frac{\partial f}{\partial y}$$

as the change is in the y direction; a vertical gradient is given by

$$\nabla f = \frac{\partial f}{\partial x} + 0$$

as the change is in the x direction. The magnitude of the gradient is given by

$$\|\nabla f\| = \sqrt{\left(\frac{\partial f}{\partial x}\right)^2 + \left(\frac{\partial f}{\partial y}\right)^2}$$

and is calculated for every pixel in the image.

3 - Non-maximum suppression

Once the gradient magnitude calculation is performed on each pixel, its value is then verified to determine whether it assumes a local maximum in the gradient direction. The gradient direction is given by

$$\theta = \tan^{-1} \left(\frac{\frac{\partial f}{\partial y}}{\frac{\partial f}{\partial x}} \right)$$

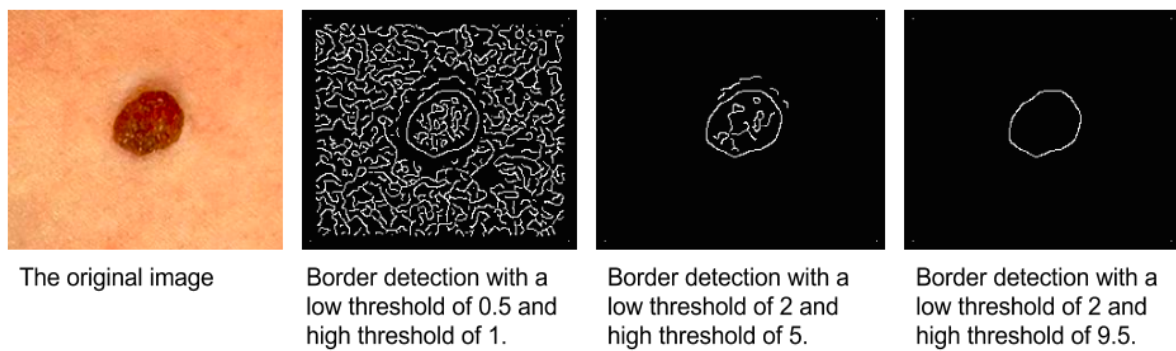
The implementation of the algorithm does not compute the gradient direction so as to avoid performing a division calculation. Instead, the two derivatives are checked for the same sign and then the largest of the two derivatives is singled out. The pixel magnitude is then compared to its two neighbor's values in the four possible directions, these being north - south, east - west, northeast - southwest and northwest-southeast. Linear interpolation is used between the two neighbor pixels for greater accuracy. Only local maximums will be considered edge candidates, therefore if the central pixel's magnitude is not greater than that of its two neighbors it will be 'suppressed' by setting its edge strength value to zero.

4 - Hysteresis thresholding

The pixels that correspond to a local maximum and in effect possess a high edge strength value are set aside as the edges detected in the image. Yet the

selected edge pixels can be further refined through specifying a threshold as the final comparison to determine an existing edge. Hysteresis thresholding is done using a low and a high threshold. The low threshold detects weak edges and the high threshold the strong edges. It was necessary to experiment to determine the optimal combination of thresholds for the situation in question, that of singling out the skin lesion in the image.

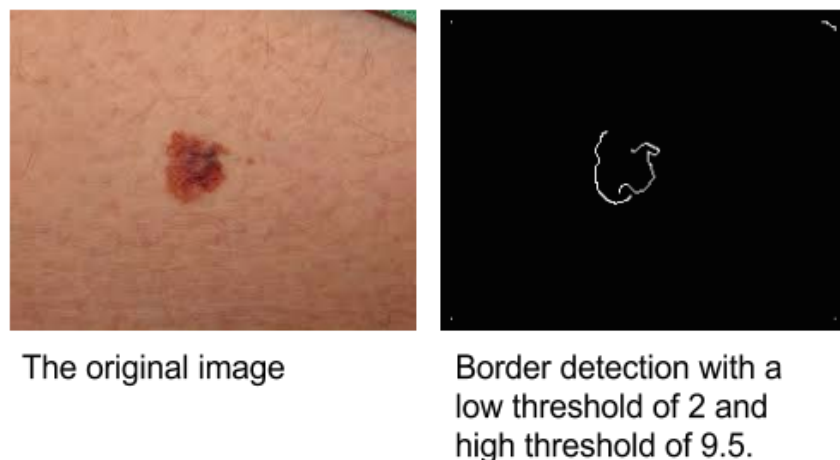
Figure 4 - Threshold performance comparison



Source: Testing performed on March 2nd, 2014.

The low threshold detected texture traces and fine edges; as the skin lesion has a considerably distinct edge a high threshold was proven to be the most adequate. With melanoma lesions the contour is not continuous; this of course is expected due to the lesion's characteristic asymmetry, border irregularity and color change. Ergo, it is presumed that this will not be misleading in the final results.

Figure 5 - Threshold performance on image of melanoma



Source: Testing performed on March 2nd, 2014.

During the course of testing, it became apparent that the algorithm as it is will only function properly if applied to images with a single lesion. Additionally, the images may need to be adapted to eliminate non-skin elements. In Figure 5, the original image shows what appears to be the hem of an item of clothing in the upper right corner. This is classified as a strong border as displayed in the image tracing the detected borders; if not treated, it will be inaccurately handled as part of the skin lesion in the subsequent phases of the algorithm.

The implementation of the Canny Border Detector developed by Tom Gibara was slightly modified so as to return a list of coordinates of the detected edge pixels as opposed to an image of the traced edges.

4.3 AB*CD Metrics

4.3.1 Asymmetry metric

Asymmetrical skin growths, in which one part is different from the other, may indicate melanoma.[29]

Symmetry is defined as invariability regardless of transformations. It is an absolute characteristic and cannot be measured in degrees. Due to this most rigid definition, rarely if ever is it possible to label a figure as symmetrical. As the images to be analyzed are of the human body, it is safe to assume that all the figures will be asymmetric. Instead of defining a figure as symmetric or asymmetric, the asymmetry will be measured and compared to an established threshold.

Symmetry in medical imaging has played an important role in contributing to diagnosis in other fields of medicine. An example of this is measuring asymmetry on mandibles from children with cleft lip and palate and children with plagiocephaly syndrome[10], measuring the asymmetry of the hippocampi to classify schizophrenic patients[10] and using the asymmetry principle in the detection of breast tumors[14].

In examining skin blemishes, rotation and reflection symmetry is of greater relevance. Two of the more recent rotation/reflection symmetry detection algorithms are G. Loy and J. Eklundh's Detecting symmetry and symmetric constellations of features[16] and V. Prasad and L. Davis's Detection rotational symmetries[25]. G. Loy and J. Eklundh's algorithm is feature based; it uses pairwise matching and voting for symmetry foci in a Hough transform to identify asymmetry. V. Prasad and L. Davis created an algorithm that filters in an input color image into a gradient vector flow field, extracting and matching the features into the gradient vector flow field, using a voting scheme for symmetry detection.

A comparative analysis of both algorithms[4] shows that the first algorithm has a higher sensitivity rate than the second; however it also presents very high false-positive rates which are of serious consequence in the medical field.

Tom Gibara's Symmetry Detection Algorithm[9] provides a method to measure asymmetry using a comparative threshold to identify rotational symmetries, more easily applicable to the analysis of the skin blemishes.

The algorithm proceeds as follows:

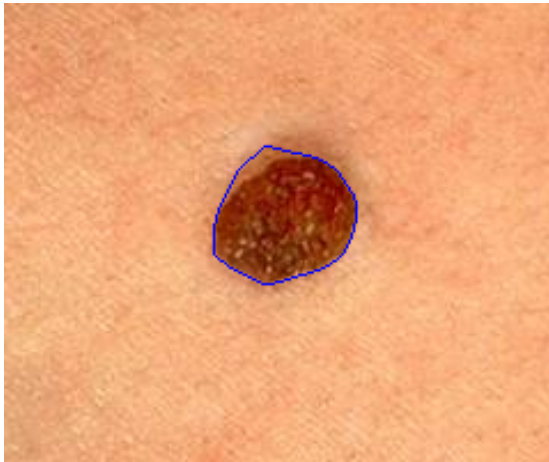
1. Identify the centroid of the object.
2. Measure the object radius (distance from centroid to most distant object pixel).
3. Choose a set of circles centered on the centroid with radius less than the object radius.
4. Sample the image at a fixed angular resolution (an even number of equiangular points) to create a vector of pixel values for each circle.
5. 'Convolve' each vector with itself to create a new set of vectors. These loosely measure the reflectional symmetry across the angle associated with each element.
6. Sum all of the resulting vectors to obtain an overall symmetry score for each angle considered.
7. Disregard any angle that does not exceed a predetermined threshold and which is not a local maximum.
8. Of the remaining angles, calculate the score-weighted average of adjacent angles (subject to a predefined threshold).
9. The resulting angles, together with the centroid, define a set of axes along which reflectional symmetry is high.

Source: GIBARA, TOM. [9]

Before running the Symmetry Detector on the images, it is necessary to delimit the region to be examined. The border traced by the Canny Edge Detector will likely not provide a continuous contour for images of melanoma lesions as they are generally multi-colored and without distinct borders (See *Figure 5*). As it happens, there is no guarantee that even the analysis of benign lesions will result in a continuous contour.

The solution to this issue is found in Yuri Pourre's implementation of the Quick Hull algorithm[24], which draws the smallest polygon possible given a set of coordinates. Once the Canny Edge Detector is run on the image, the resulting list of coordinates of the detected edge pixels is fed into the Quick Hull program.

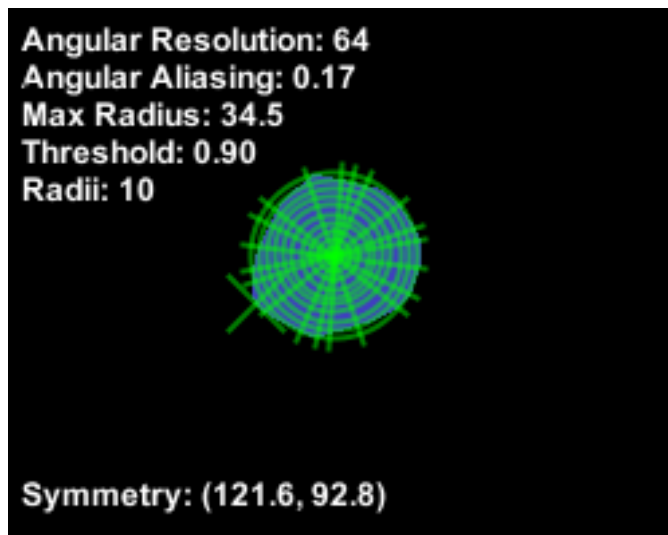
Figure 6 - Quick Hull generated polygon containing the skin lesion



Source: Testing performed on March 9th, 2014.

An image with the polygon outline is then filled in and converted to grayscale for compatibility with Gibara's Symmetry Detector algorithm. The important algorithm parameters[9] are Angular Resolution, Angular Aliasing, Radius Count ('Radii' in the sample output in Figure 8), and Threshold. The Angular Resolution is the number of sample arcs in the circle. Angular Aliasing is the smallest angle permitted between identified axes of symmetry. Angles closer together than this value are combined into a single angle. Radii indicates the number of different radii at which samples are taken. Threshold is the proportion of the maximum possible score that an angle must obtain to be considered. Once the detector is run, a summary of the execution is displayed. The above parameters and their respective values are listed. Blue pixels indicate pixels identified with the object, in this case the polygon surrounding the skin lesion. The green 'plus' indicates the position of the centroid, currently not visible due to the many traced lines of reflectional symmetry. The green 'cross' indicates a pixel at maximum distance from the centroid. Green circles indicate the circles from which samples of image data were taken. Green lines indicate the lines of reflectional symmetry identified by the algorithm.

Figure 7 - Summary of Symmetry Detector results



Source: Testing performed on March 9th, 2014.

4.3.2 B - Border Irregularity metric

Melanomas may have borders that are vaguely defined. Growths with irregular, notched or scalloped borders need to be examined by a doctor[29].

As benign lesions are of a circular nature, it is expected that the radius of the lesion will be constant, or more specifically very nearly so, throughout the lesion. The logic behind the calculation of this border irregularity metric is very straightforward. Succinctly, it entails calculating the coefficient of variance of the lesion's radii.

1. A list of coordinates of the lesion's border is obtained from the Canny Corner Detector;
2. The centroid of the lesion would be calculated by finding the mean x and y values; however as the contour of melanoma lesions is not continuous, it was necessary to correct this formula. The coordinates of the centroid are the minimum value x and y plus an offset of the difference between the maximum and minimum value of x and y divided by 2.

$$C_x = x_m + (x_M - x_m)/2 \quad C_y = y_m + (y_M - y_m)/2$$

3. The mean radius is obtained by calculating the average of the Euclidean distance between the centroid and each point in the list of border coordinates;

4. The standard deviation is given by

$$\sigma = \sqrt{\frac{1}{n} \sum_{i=1}^n (r_i - \bar{r})^2}$$

with n as the number of coordinate pairs (points) in the list, r_i as the radius at point i and \bar{r} as the mean radius. Bias correction is unnecessary given the sample is equal to the population.

5. Obtain the coefficient of variance given by

$$c_v = \frac{\sigma}{\mu}$$

being that μ is the mean radius calculated in step 3.

Figure 9 - Comparison of metric on malignant and nonmalignant lesions

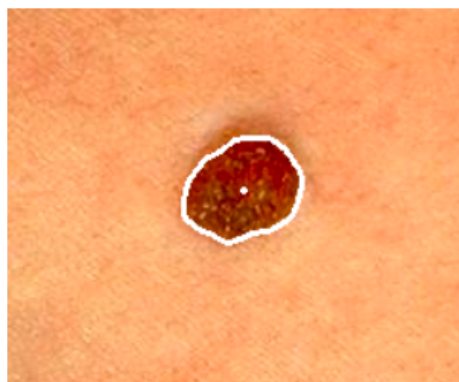


Image of a benign growth and the tracing in white of the detected edge and centroid.
Border Irregularity metric: 0.107



Image of a melanoma lesion and the tracing in white of the detected edge and centroid.
Border Irregularity metric: 0.132

Source: Testing performed on March 5th, 2014.

4.3.3 C - Color Changes

Multiple colors or uneven distribution of color may indicate cancer.[29]

Depending on the resolution and lighting of the image taken of the skin lesion, color variance may be noticeable even in benign lesions. This makes it necessary once again to measure the difference between colors in the lesion and compare this difference to a defined threshold. The difference between colors is represented by Delta-E, a metric established by the International Commission on Illumination to quantify color differences. Using this metric, the algorithm will be quite

straightforward:

1. Identifying the lesion within the image using the Canny edge detector;
2. Calculating the Delta-E of the selected portion of the image;
3. Establish a color change threshold using a tree model;

Functions to perform the Delta-E calculation are included in many existing image manipulation libraries. The Delta-E measure can then be compared to the threshold to assist in the final diagnosis.

2.3.4 D - Diameter greater than 6mm

A skin growth's large size may be an indication of cancer.[29]

This final criteria presents a challenge for the application of computerized image analysis; the images will be taken at different ranges with no comparative figure, impairing an accurate calculation of real size. A proposed solution is to identify the pores in the image and measure the average distance between them in pixels; this would provide a scale of the lesion's diameter. An adaptation of Q. Zhang and T. Whangbo's Skin Pores Detection Algorithm[28] will be implemented to find the pores in the image and note their coordinates so as to determine the distance between them. The algorithm is based on image segmentation. A preprocessing algorithm to balance the illumination of the image must be run before the pore detection algorithm. The Global Luminance Proportion algorithm is noted below.

Using the original image of MxN size:

1. a. Calculate the average luminance of the image;
- b. Split the image S into V sub-blocks, calculating the average luminance;
- c. Obtain luminance difference matrix D;
2. Interpolation algorithm for matrix D until element number in matrix equals MxN;
3. Merge matrix D and original image S into new image sized MxN.

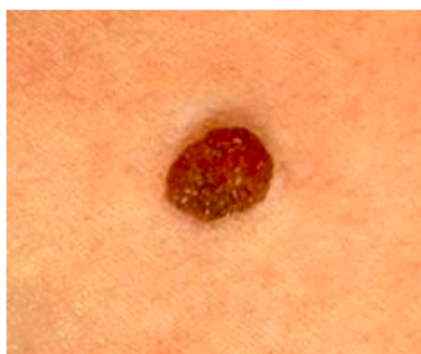
When the image has balanced luminance, the segmentation is performed using the Fuzzy C-Means Algorithm. After this segmentation, pixels in the image are labeled to 8 connectivity and skin pores can be classified from the 8-connectivity labeled image by calculating the quadratic moment and the ration between row and column moments.

2.2.5 Image pre-processing

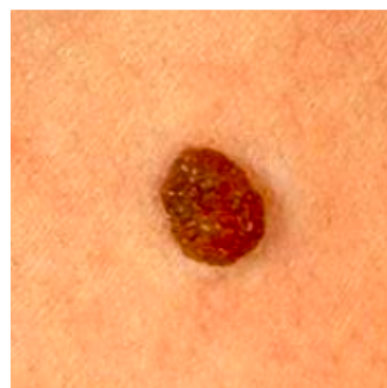
In preparation for processing, each of the images is run through an application that rotates the image 30° counter-clockwise a total of 12 times, storing a copy of the image after each rotation. This is done by suggestion of prof. Rob Fergus as a strategy to boost the image dataset to be used in the evaluation of the algorithms. The files of the rotated images are named after the original image ID for control purposes, see Figure 2.

Figure 2 - Image rotation

File 0010.png



File 0010-3.png



Original file 0010.png and processed image 0010-3.png,
representing the image after 3 consecutive rotations of 30° .
Image source: www.onecaremedicalcenter.com

Source: Processing performed on the 22nd of February 2014

References

- [1] ABASSI, Naheed R. et al. Early Diagnosis of Cutaneous Melanoma: Revisiting the ABCD Criteria. **Journal of the American Medical Association**, December 8, 2004, Vol 292, No. 22
- [2] ANEJA, S; ANEJA, S; BORDEAUX J.S. **Association of Increased Dermatologic Density With Lower Melanoma Mortality**. Case Western Reserve University, Yale University School of Medicine, 2012.
- [3] CANNY, John. **A Computational Approach to Edge Detection**. IEE Transactions on Pattern Analysis and Machine Intelligence, Vol. PAMI-8, NO. 6, November 1986.
- [4] CHEN, Po-chen et. al. **A Quantitative Evaluation of Symmetry Detection Algorithms**. 17 pages. Penn State University & Carnegie Mellon University, 2007.
- [5] CLAWSON, K.M. et al. **Analysis of Pigmented Skin Lesion Border Irregularity Using the Harmonic Wavelet Transform**. Machine Vision and Image Processing Conference, 2009. IMVIP '09.
- [6] DAUBECHIES, Ingrid. **Where do wavelets come from? - A personal point of view**. Department of Mathematics and Program in Applied and Computational Mathematics, Princeton University.
- [7] FRIEDMAN, R. J.; RIGEL, D. S.; KOPF, A. W. Early Detection of Malignant Melanoma: The Role of Physician Examination and Self-Examination of the Skin. **CA Cancer Journal for Clinicians**. 1985 May-Jun;35(3):130-51
- [8] GIBARA, Tom. **Canny Edge Detector Implementation**. Available at: <http://www.tomgibara.com/>. Accessed on January 23rd, 2014.
- [9] GIBARA, Tom. **Symmetry Detection algorithm**. Available at: <http://www.tomgibara.com/>. Accessed on January 23rd, 2014.
- [10] GLERUP, Nanna. **Asymmetry measures in medical image analysis**. 174 pages. Department of Innovation, IT University of Copenhagen, 2005.
- [11] JING, Li et al., Brief Introduction of Back Propagation (BP) Neural Network Algorithm and Its Improvement. **Advances in Intelligent and Soft Computing** Volume 169, 2012, pp 553-558

- [12] JORGENSEN, P.E.T.; SONG, M.-S. **Comparison of Discrete and Continuous Wavelet Transforms**. Springer Encyclopedia of Complexity and Systems Science, Springer, 2008.
- [13] KIMBALL, A.B.; RESNECK, J.S. The US dermatology workforce: a specialty remains in shortage. *Journal of the American Academy of Dermatology*, 2008 Nov; 59(5):741-5.
- [14] KURUGANTI, P.T.; HAIRONG, Qi. **Asymmetry analysis in breast cancer detection using thermal infrared images**. Engineering in Medicine and Biology, 2002. 24th Annual Conference and the Annual Fall Meeting of the Biomedical Engineering Society EMBS/BMES Conference, 2002. Proceedings of the Second Joint.
- [15] LEE, Tim K. et al. **Irregularity index: A new border irregularity measure for cutaneous melanocytic lesions**. Vancouver: Elsevier, 2003.
- [16] LOY, G.; EKLUNDH, J. **Detecting symmetry and symmetric constellations of features**. European Conference on Computer Vision (ECCV'04), Part II, LNCS 3952, pages 508,521, 2006.
- [17] MA, L.; STAUNTON, R.C. **Analysis of the contour structural irregularity of skin lesions using wavelet decomposition**. Hangzhou Dianzi University & University of Warwick, 2012.
- [18] MA, Zhen et al. **A review on the current segmentation algorithms for medical images**. 6 pages. Faculty of Engineering, University of Porto.
- [19] McKOY, Karen. **The Importance of Dermatology in Global Health**. Harvard Medical School Department of Dermatology.
- [20] MONTEIRO, Fábio. Saúde privada não consegue administrar o aumento da procura. **Correio Braziliense**, May 2011.
- [21] Morlet, J. et al. Wave propagation and sampling theory. **Geophysics**, VOL. 47, NO. 2, Pages 203-221, February 1982.
- [22] NACHBAR, Franz et al. The ABCD rule of dermatoscopy. **Journal of the American Academy of Dermatology**, Volume 30, Issue 4 , Pages 551-559, April 1994.
- [23] NEWLAND, David E. **Harmonic Wavelet Analysis**. Department of Engineering, University of Cambridge, 1993.
- [24] POURRE, Yuri. **Quick Hull Algorithm**. Available at: <<https://github.com/yuripourre/>>. Accessed on March 5th, 2014.

- [25] PRASAD, V.;DAVIS, L. **Detection rotational symmetries.** IEEE International Conference on Computer Vision (ICCV), pages 346–352, 2005.
- [26] RICOTTI, Charles et al., Malignant Skin Neoplasms. **Medical Clinics of North America**, Vol. 93, Issue 6, Pages 1241-1264
- [27] THOMAS, L. et al., **Semiological Value of ABCDE Criteria in the Diagnosis of Cutaneous Pigmented Tumors.** Unité de Dermatologie et Département d’Informatique Médicale des Hospices Civils de Lyon, Hôpital de l’Hôtel-Dieu, Lyon, France Dermatology, 1998.
- [28] ZHANG, Qian; WHANGBO, Taeg Keun. **Skin Pores Detection for Image-Based Skin Analysis.** 5 pages. Department of Computer Science, Kyungwon University, 2008.
- [29] **Melanoma pictures to help identify skin cancer.** Available at: <<http://www.mayoclinic.com/health/melanoma/DS00575>>. Accessed on October 19th 2013.